ScienceDirect
www.sciencedirect.com

Fusion Engineering and Design 00 (2021) 1–12

R I A I
www.elsevier.es/RIAI

Liquid metal MHD flow influence on heat transfer phenomena in fusion reactor blankets

Daniel Suarez*, Eduardo Iraola, Cristina Lampón, Elisabet Mas de les Valls, Lluis Batet

Departament de Física, Universitat Politècnica de Catalunya, Barcelona, Spain

Abstract

DEMO reactor is projected as a technological demonstrator and a component test reactor for several key systems such as the breeding blanket. The dual coolant lithium lead (DCLL) is one promising breeding blanket candidate that performs the functions of shielding, part of the cooling and breeding with the same liquid metal fluid. PbLi is also in charge of transporting the bred tritium to the Tritium Extraction System. Structural cooling of the blanket walls is performed by pressurized helium flow which also transfers heat to the balance of plant. Keeping a proper distribution of thermal loads between the two coolants is a key aspect to reach a plant high efficiency. The thermal power transferred from the liquid metal to the helium channels depends on the flow regime. While liquid metal flows under the magnetic field, the magnetohydrodynamic (MHD) phenomena will occur, influencing the flow regime and the velocity profile. The heat is volumetrically deposited in the liquid metal coolant due to the interaction between the highly energetic neutrons originated in the plasma and the coolant. The heat deposition profile is roughly exponential causing temperature differences across the same channel cross section. Temperature gradients induce buoyant effects altering the expected MHD profile and affecting the heat transfer rate from the liquid metal to the surrounding walls cooled with helium. It is of utmost interest to identify the effects of the main flow parameters on the heat transfer coefficient under such complex conditions. The work studies computationally a domain consisting of a liquid region and a surrounding solid region electrically and thermally coupled using latest EU DCLL design characteristics. A fully developed flow is assumed where buoyancy is modelled under the Boussinesq approximation. Joule effect has been considered negligible compared to the neutron deposition. The influence of the buoyant MHD phenomena to the heat transfer coefficient is analysed parametrically with a CFD solver implemented in OpenFOAM®. The parameters investigated here are the Reynolds, Hartmann and Grashof numbers, the Grashof ratio, and the wall conductance ratio (c_w).

Keywords: Magnetohydrodynamics, Heat transfer, Breeding Blanket, DCLL, EU-DEMO, Computational Fluid Dynamics

1. Introduction

The breeding blanket (BB) will be a key component of Tokamak type fusion nuclear power plants. Dual-coolant lead-lithium (DCLL) is one of the BB designs considered within EU DEMO project as advanced blankets [1] [2]. In DCLL, pressurized He will cool the structure while the liquid metal (LM) will perform the following three functions: extract the volumetric heat deposited in the breeding channels (cooling), breed the tritium from the neutron-lithium interaction, and shield the tokamak's magnetic coils from the neutron radiation.

The CIEMAT laboratory is in charge of the EU-DCLL design and its latest proposal consists of a single-module segment (SMS) allowing the PbLi to reach high temperatures (above $550°C$), enhancing the balance of plant (BOP) efficiency. Details on the latest design can be found on [3] and [4].

One of the features of such new design is that PbLi will flow upwards in all the channels in the BB, preventing the buoyant MHD reverse flow phenomena expected in rear channels of the multi-module segment previously proposed [5]. This feature will contribute to vanish recirculating zones where the fluid can become stagnant and tritium and temperature can build up. This contributes, therefore, to a stabilization of the flow streamlines along the channels: vortexes will only be expected when buoyant or inertial forces overcome viscous forces on the MHD side layer next to the first wall. The walls containing the PbLi fluid are expected to be made of a ceramic insulating material,

*Corresponding author: daniel.suarez.cambra@upc.edu

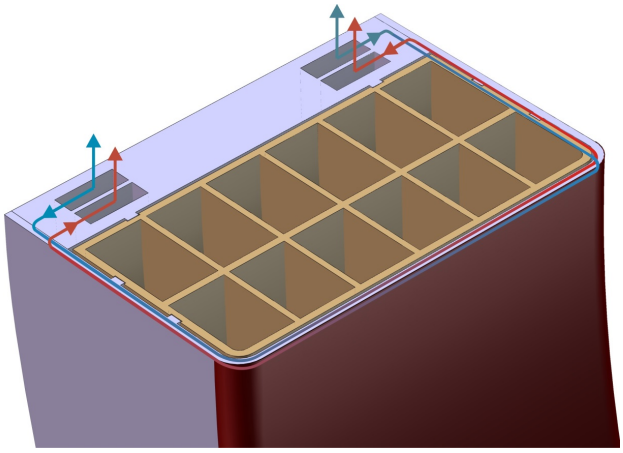

Figure 1: Single-module segment PbLi twelve channels cross-section. Arrows refer to the helium coolant flow [3]

avoiding the electric coupling between fluid and surrounding structure.

Figure 1 shows the twelve PbLi channels on a SMS. The red (right) part corresponds to the first wall.

The PbLi flow regime can be classified as mixed convective flow, combining the forced and natural convection due to buoyancy. The different ratios between forces affecting the fluid (inertial, characterized by the Reynolds number, buoyant, characterized by the Grashof number, and magnetic, characterized by the Hartmann number) will determine the flow velocity profile, and will determine too whether the flow is fully-developed (with straight streamlines) or vortexes are to be expected.

The understanding of the flow velocity profile is of most importance since it has the greatest influence on heat, mass and momentum transport phenomena.

In 1997, Ji et. al. [6] presented their study on the influence of the turbulence damping by the MHD phenomena on the heat transfer in a heated horizontal circular pipe with a uniform external magnetic field. The study presents an empirical correlation for the averaged Nusselt number as a function of the Peclet and Hartmann numbers.

Barleon et. al. in 2000 [7] studied experimentally the heat transport phenomena in rectangular channels with one heated wall for insulating and conducting walls. Morley et. al., the same year [8] reviewed previous works on the influence of the M-shaped jets on the temperature distribution.

In 2002 Tagawa et. al. [9] numerically analyzed the 2D buoyant MHD flow in an infinite vertical channel with a temperature gradient perpendicular to the magnetic field. In 2003, Authié et. al. [10] analyzed the 3D buoyant MHD flow in a vertical limited enclosure, and showed experimental results.

In 2008 [11] and in 2009 [12] the UCLA group obtained interesting results regarding the establishment of the quasi-two-dimensional (Q2D) flow regime in vertical buoyant channels, such as DCLL's. In this case the 2D domain was a vertical plane, perpendicular to the magnetic field, using the Q2D formulation proposed in [13].

Several studies have analyzed the temperature distribution in a vertical channel flow without considering the buoyancy phenomena. Some examples were used to study the influence of the Flow Channel Insert in DCLL BB [14] [15] [16]. A recent relevant work developed at PPPL calculated the non-buoyant heat transport at DCLL blanket with a magnetic vector potential approach, and included the helium flow influence on such heat transport. [17]

In an internal EUROfusion report [18], two 3D magneto-convective cases were analyzed. They shared the Reynolds ($Re = 5000$) and Hartmann ($Ha = 120$) dimensionless numbers but they differ in the Grashof number. On the one hand, the $Gr = 10^8$ reproduced one of the cases analyzed in [11]. The 3D analysis showed, as the authors in [11] stated, that the Q2D model underpredicted the onset of instabilities. On the other hand, a case with $Gr = 3 \cdot 10^6$ was calculated, and results showed a fully developed condition. Although the fully developed condition is only obtained under certain ranges of dimensionless ratios that are yet not fully known, the latter result gives grounds for the use of the fully developed hypothesis in a 2D magneto-convective model using similar dimensionless numbers.

Recently, in 2020, an outstanding work in UCLA regarding the buoyant 3D MHD flow phenomena and its numerical simulation using their HIMAG code was published [19]. Similarly to [18], it showed that the range of selected dimensionless numbers determine the flow regime. The work investigated the influence of Gr, Ha and Re on the velocity profile, the turbulence intensity and the departure from Q2D turbulence regime.

According to the referenced works, three methods may be used to study computationally the buoyant MHD flow behaviour. One is the 3D buoyant code, which is the most precise but also the most expensive in terms of computational resources, what justifies that the presented studies are far from the DCLL conditions ($Ha \sim 10^4$ and $Gr \sim 10^{12}$), what corresponds to a Lykoudis number of $Ly = Ha^2/Gr^{0.5} \sim 10^2$. The Lykoudis number is commonly used to measure the ratio of the Lorentz forces over the buoyant forces. Another method is the use of Q2D codes, that may represent the 2D vorticity generated by the combination of buoyancy and magnetic fields. This method is very useful since it is computationally affordable but gives no information in the plane perpendicular to the flow direction and therefore the Hartmann boundary layer is not simulated. The last method is to use a 2D fully developed buoyant MHD code. This method is as affordable as the Q2D, gives very detailed information of the distribution of temperatures in the plane perpendicular to the flow direction, but is not capable to reproduce any instability at all, since the flow direction is forced to be fully-developed. Using a fully-developed model for flow regimes where the flow is of 3D nature would yield nonphysical results.

The work presented here analyzes the heat transfer phenomena based on the co-planar distribution of temperature

using a 2D magneto-convective fully-developed code.

This work is divided in four parts as follows: the first one is devoted to describe the characteristics of the fully developed flow model that will be used to study the heat transport in a DCLL front central channel; the second part will present the results of the benchmark case used to test the fully-developed buoyant MHD code; the third part will explain the work done on the optimization of the code performance and its results; and the fourth part explains the application of the optimized code to the DCLL channel model (described in the first part) and a sensitivity analysis performed with different dimensionless numbers.

In the sensitivity analysis, the influence of some dimensionless parameters (from now on 'variables') in heat transport has been studied through the analysis of some 'parameters of interest'. The selected dimensionless parameters (variables) have been Hartmann number, Reynolds number, Grashof number, Grashof ratio and wall conductance ratio (c_w). The selected 'parameters of interest', that have been chosen because of their significance on the breeding blanket performance, are: Nusselt number, maximum dimensionless vorticity, maximum dimensionless velocity, maximum temperature in the fluid and in the surrounding wall, maximum thermal gradient on the wall and dimensionless pressure drop.

The way the sensitivity analysis has been designed establishes a work methodology to capture the influences of the variables over the parameters of interest. The next step in the research line will be to understand the flow regimes associated to certain ranges of such variables. It will clarify, under which of those ranges, the 2D fully developed approach may be used. Finally, in future works, the methodology used in the present report will be applied closer to the limits where the 2D fully-developed assumption is valid.

2. Description of the fully developed model

The studied channel is a vertical enclosure with ceramic walls with negligible electrical conductivity according to the latest CIEMAT DCLL design [3]. The model represents a central front channel of the SMS shown in Figure 1. The dimensions can be seen in Figure 2, as well as the directions of the magnetic field (B), the flow (U), and the heat flux (Q_W). There is also a volumetric exponential heat generation (Q_G) as shown in the figure. The domain has been halved and the symmetry plane is shown with a discontinuous line. Symmetry in the plane perpendicular to the magnetic field direction is a consequence of the symmetric electric currents and velocities seen in previous calculations [20]. The red region is the ceramic wall and the blue is the lead-lithium liquid flow.

The plasma is further in the right side of the figure, but between the plasma and the DCLL channel there is an EUROFER wall with internal helium cooling channels that will effectively extract heat from the lead-lithium channel (Q_W). This helium cooling of the first wall is considered to remove any direct surface heating by the plasma as well as to extract some heat generated inside the liquid domain. The heat flux Q_W only applies to one side since the domain corresponds to a central front channel of the SMS.

The flow is considered to be buoyant and fully-developed, therefore a 2D set of equations has been considered and only the velocity component perpendicular to the channel cross-section has non-zero value. The induced magnetic field is considered negligible compared to the externally applied magnetic field from the tokamak coils (low magnetic Reynolds number).

The set of equations applied for this study are the Navier-Stokes equations coupled to the Maxwell equations. The flow is considered incompressible and the buoyancy is modeled in the momentum equation using the Boussinesq hypothesis. The current density conservative scheme [21] suits perfectly with the low magnetic Reynolds number of the case, which justifies the use of the inductionless approximation and the so-called ϕ-formulation, i.e.:

$$\nabla \cdot \mathbf{v} = 0 \tag{1}$$

$$\frac{\partial \mathbf{v}}{\partial t} + (\mathbf{v} \cdot \nabla)\mathbf{v} = -\frac{\nabla p}{\rho} + \nu \nabla^2 \mathbf{v} + \frac{\mathbf{j} \times \mathbf{B}}{\rho} + \beta \theta \mathbf{g} \tag{2}$$

$$\nabla^2 \phi = \nabla \cdot (\mathbf{v} \times \mathbf{B}) \tag{3}$$

$$\mathbf{j} = \sigma_m(-\nabla \phi + \mathbf{v} \times \mathbf{B}) \tag{4}$$

$$\frac{\partial \theta}{\partial t} + \nabla \cdot (\mathbf{v}\theta) = \alpha \nabla^2 \theta + S_{th} \tag{5}$$

where v is fluid velocity, t time, p pressure, ν kinematic viscosity of the fluid ($\nu = \mu/\rho$), j electric current density, ϕ electric potential, σ_m electric conductivity of the fluid, B external magnetic field, β the Boussinesq thermal expansion coefficient, θ is the co-planar temperature difference between each cell temperature T_i and the average temperature of the bulk in the 2D domain ($\overline{T}_b$) so that $\theta = T_i - \overline{T}_b$, g is the gravity acceleration constant, $\alpha = k_{th}/(\rho \cdot C_p)$ is thermal diffusivity, k_{th} is thermal conductivity and C_p is specific heat.

The studied fluid is PbLi and its relevant physical properties can be retrieved from Mas de les Valls [22] evaluated at $400°C$, and from a more recent work from Martelli et. al. [23]. The wall material is silicon carbide (SiC) as proposed in [3]. Although most properties are temperature dependent, they have been considered constant since the analysis corresponds to a fluid cross-sectional plane. They are shown in Table 1.

	PbLi	SiC [3]
$\rho\ (kg \cdot m^{-3})$	9720 [22]	3100
$\sigma\ (S \cdot m^{-1})$	$7.63 \cdot 10^5$ [22]	depends on c_w
$\mu\ (Pa \cdot s)$	$1.49 \cdot 10^{-3}$ [22]	-
$C_p\ (J \cdot (kg \cdot K)^{-1})$	189 [22]	670
$\kappa\ (W \cdot (m \cdot K)^{-1})$	22.36 [23]	125
$\beta\ (K^{-1})$	0.00012 [23]	-

Table 1: Physical properties of the materials

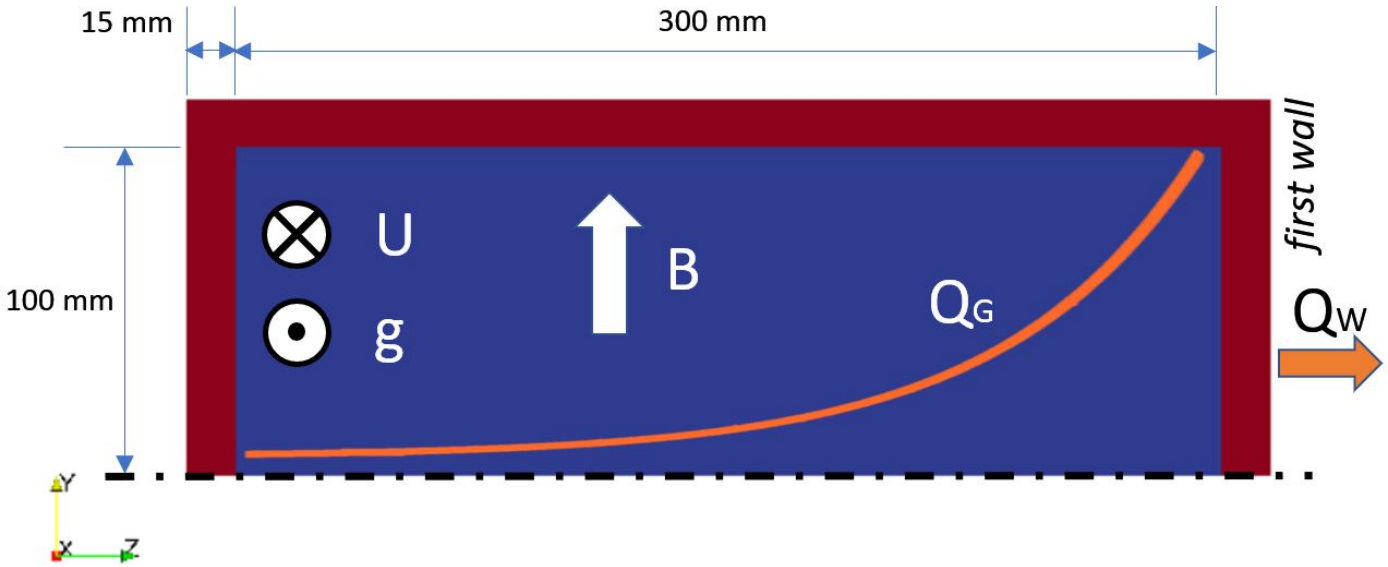

Figure 2: Studied domain: half channel cross-section. Blue region is PbLi and red region is ceramic wall

The momentum balance is affected by the temperature difference in the plane only through the buoyant term. The source term S_{th} is linked to the volumetric heat deposition coming from the neutron flux, and will be explained later. The Joule dissipation by the electric currents have been omitted as it is considered negligible compared to the neutron deposition heat source [24].

All these equations are solved for the liquid region. Only Equations 3, 4 and 5 are solved also for the solid region, considering the physical properties of the solid wall. A detailed derivation of this set of equations and the PISO-like solution procedure using a finite volume approach can be found on Mas de les Valls [20] and on Ni et al. [21]. The code was named ϕ-MHDFoam.

The dimensionless numbers (the problem variables) that describe the case are five: the Hartmann number ($Ha = Bb\sqrt{\sigma_m/\mu}$), the Reynolds number ($Re = \rho v D_h/\mu$), the wall conductance ratio ($c_w = \sigma_w t_w/\sigma_m b$), the Grashof number ($Gr = g\beta\Delta T a^3/\nu^2$), and the Grashof ratio ($GrR = Q_W/Q_G$). Parameters σ_w and t_w correspond to wall electric conductivity and wall thickness, a is half width of the channel in the heat flux radial direction, b is half width of the channel in the magnetic field direction and D_h is the hydraulic diameter. Q_W stands for the heat flux through the outer wall (first wall).

The temperature difference ΔT is originated by Q_G, a non-uniform (exponential) volumetric heating only of the liquid metal caused by neutron flux interaction as described in [25]. The wall region is considered to have no volumetric heating. By convention, the Gr number definition determines the ΔT, and it is used to size the mean volumetric heat generation with $\overline{q} = k \cdot \Delta T/a^2$. Total heat generation is $Q_G = \overline{q} \cdot V$. The heat deposition is modeled as an exponential profile shape, then $Q_G = \int_V q_0 \cdot e^{-mz} \cdot dV$. Finding q_0 allows to find the source term:

$$S_{th} = S_0 \cdot \mathrm{e}^{-m \cdot z} \tag{6}$$

where $S_0 = q_0/(\rho \cdot C_p)$. $z = 0$ corresponds to the center of the channel width in the z direction as shown in Figure 2.

The numerical strategy is to compute a cyclic inlet and outlet boundary condition for the velocity, the θ and the electric potential fields with one node in the flow direction. The velocity at walls is zero and the non-slip condition has been imposed. The flow rate is maintained according to the desired Re number, characterized by the mean cross-sectional velocity U, by adjusting the source pressure gradient term. The magnetic field B is fixed and imposed according to the Ha number and applies to all domain. External walls are electrically insulated, thus, the electric potential field has zero gradient boundary condition. The electric potential extends throughout all the domain, i.e. the wall and the fluid regions are electrically coupled guaranteeing the conservation of normal current and electric potential at the solid/fluid interface. The thermal gradient in the flow direction is computed using a domain energy balance so that $\partial\theta/\partial x = Q/(\dot{m} \cdot C_p \cdot L)$, with Q the net heat absorbed by the domain, L the length of the domain (in x direction) and $\dot{m}$ the mass flow rate. The boundary condition for all walls is adiabatic, except for the wall on the right hand side, next to the first wall, where a fixed gradient is imposed by the Grashof ratio (GrR).

The set of Equations 1 to 5 have been modified to calculate a fully developed flow by imposing a fixed flow rate through a uniform pressure gradient source term in the flow direction. The electric and thermal equations have been prepared to be solved through different regions, allowing fluid-solid interaction at the boundaries. The implementation was done over the OpenFOAM CFD package as detailed in Mas de les Valls [20].

The mesh used in all cases was hexahedral. The num-

ber of nodes in each boundary has been set according to the recommendations found on the detailed report by Mistrangelo [26] on the mesh refinement requirements. All meshes have 8 nodes on Ha boundary layer ($\delta_h = 2b/Ha$) and 30 nodes on the side boundary layers ($\delta_s = 3b/Ha^{0.5}$). The cell growing criteria has been set so that the cell to cell expansion ratio is 1.05 maximum. A detail of the mesh used for cases with $Ha = 3000$ can be seen in Figure 3.

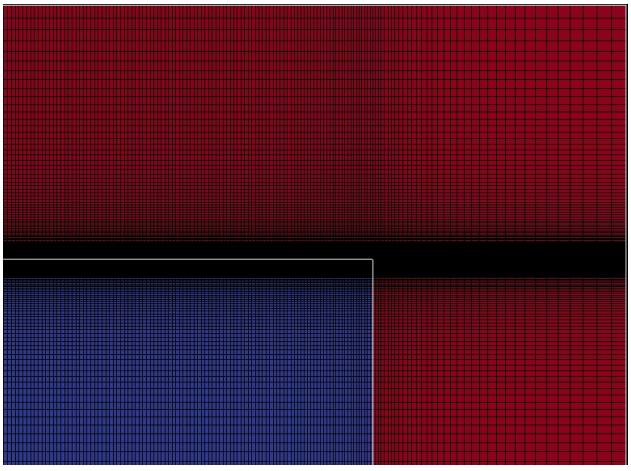

Figure 3: Detail of the mesh on the top right corner for $Ha = 3000$ cases. The white line represents the boundary between fluid and wall

Selected discretization schemes were central differencing, of second order, and the steady state was considered reached when $(\psi^i - \psi^{i-1})/(\psi^{i-1} \cdot \Delta t) < 10^{-6} s^{-1}$, with the variable of interest ψ being the maximum temperature in the fluid and Δt the time-step size.

Before detailing the characteristics of the studied cases and the parameters of interest, the code has been validated with a benchmark case. The benchmark case has been used to optimize the solver for buoyant MHD cases, and the result of such optimization is also shown.

3. Code Validation

Although the multi-material electric and thermal coupling had already been validated in [15], the buoyant fully-developed MHD code still required its own validation. The selected benchmark case has been Tagawa's and Authié's work [9], a single-material case (without wall coupling). This formal analysis investigates the flow profile resultant in an infinite vertical channel without any pressure gradient, where a conducting fluid is affected by a magnetic field perpendicular to the channel direction and by a temperature gradient perpendicular to the former two directions (magnetic field and channel). This benchmark case resembles the configuration of the MHD flow phenomena expected in a vertical channel of the DCLL blanket, and can be seen in Figure 4. The flow is initially at rest, but once the thermal gradient is applied it buoys up in the region next to the hot wall and it falls down in the region next to the cold wall. The thermal gradient, ΔT, is set so that on the hot wall the temperature is fixed at $+\Delta T/2$ and on the cold wall at $-\Delta T/2$. ΔT is obtained using the reference Gr number.

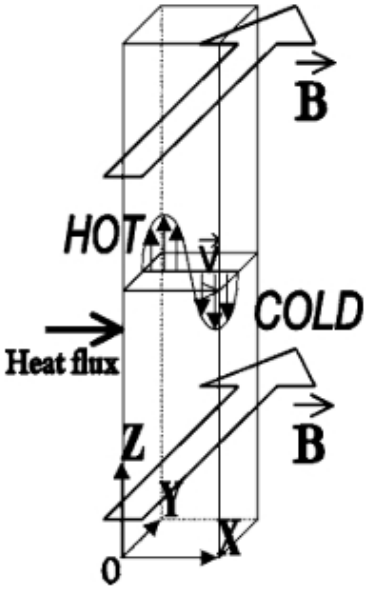

Figure 4: Configuration of the benchmark case [9]

Recirculation effects are not considered since it is an ideal infinite vertical enclosure, and whatever recirculation effect has been dumped far from the studied region. The enclosure is squared-shaped of side l=0.15 cm, that will be used as characteristic length for the relevant dimensionless numbers: Hartmann number and Grashof number. The velocity is normalized by ν/l.

The obtained dimensional velocity profile can be seen in Figure 5, and normalized U_{max} with the obtained errors are shown in Table 2. The error magnitude for different Ha number shows a successful code validation.

4. Code Optimization

The benchmark case has been used to measure the code optimization results. It consisted in:

1. Reduction from three nodes in the flow direction (old code) to only one (new code).
2. Arrange the code structure to be able to solve the case in parallel.
3. Increase the time-step size until right before the onset of magnetic Courant-Friedrichs-Levy (CFL) numerical related instabilities take place, taking advantage of the steady state condition. This time-step size constraint is carefully explained in [20].

The new code uses one row (i.e. one cell in the flow direction) while the old one uses three. The cells per row have been ~ 7500 for the $Ha = 100$ case, ~ 23000 for the

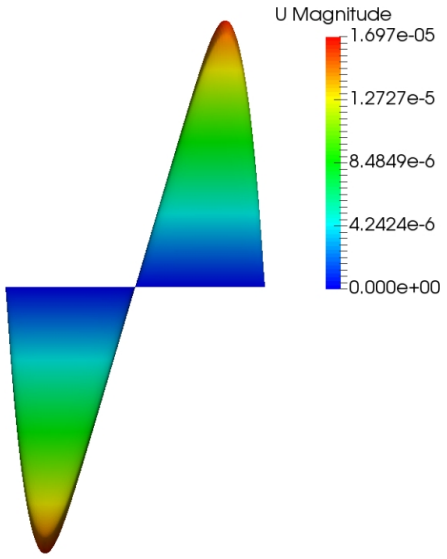

Figure 5: Velocity field result (m/s) for $Ha = 100$ and $Gr = 10^4$

Ha	U_{max}	Error(%)	Time old code (min)	Time new code (min)
100	16.55	0.72	2098	4.3
500	4.11	0.97	16413	140
2000	1.13	0.28	-	1119

Table 2: Benchmark and code optimization results

Ha	Cores	Time new code (min)	Strong scaling efficiency
100	1	4.3	-
100	2	2.2	97.7%
500	1	140	-
500	2	73.5	95.2%
2000	1	1119	-
2000	3	676.1	56%
2000	6	376.1	67.9%

Table 3: New code parallel scaling efficiency

$Ha = 500$ case and ~ 54000 for the $Ha = 2000$ case. Table 2 shows the benchmark results.

The strategy to increase the time step size before the onset of instabilities is outlined in the following lines. The algorithm used in the benchmark cases monitors the evolution of the variation of the maximum velocity in the domain, such as $\psi_U^i = (U_{max}^i - U_{max}^{i-1})/U_{max}^{i-1}$, being U_{max}^i the latest time step maximum velocity, and U_{max}^{i-1} the maximum velocity at the previous time step. In case the algorithm finds out that $\psi_U^i < \psi_U^{i-1}$ the time step size is increased by 0.5% (small enough to avoid numerical instabilities and large enough to provide the code performance improvement) and in any other case the time step size is decreased by 0.5%. A comparison of the evolution of U_{max}, ψ_U and Δt (time step size) is shown in Figure 6. In the figure, it can be observed that both solvers start the simulation with the same time step size, which corresponds to a maximum Courant number in the domain (C+D+L as defined in [20]) of 1. The solver stops the benchmark simulation after 1000 iterations with $\psi_U < 10^{-8}$.

The code optimization has been encouraging and successful. Calculation times have been dramatically reduced while the accuracy of the solver is very high. The $Ha = 2000$ case has deliberately not been calculated with the old code due to its unaffordable simulation time. Table 3 shows the strong scaling efficiency ($sse = t_1/(N \cdot t_N)$) for the benchmark case. t_1 stands for the calculation time with one processor, and t_N the calculation time with N parallel processors. The sse value for $Ha = 2000$ is very low, and although it has been revised, the reason remains unknown.

5. Application of the optimized code to a fully developed model of the DCLL blanket with sensitivity study

The selected set of values for the dimensionless variables in this study is presented in Table 4. The variables have been selected because, according to the provided references in Section 1 [18], they guarantee the fulfilment of the fully-developed assumption: the flow direction can only be perpendicular to the plane of study.

In case of the Hartmann number (~ 3000), it has been bounded by the available computational resources.

The selection of the Reynolds number is limited by the fully-developed laminar flow regime assumption. According to [27], for $Re < 65 \cdot Ha^{1/2}$ (corresponding to $Re <\sim 3500$) the Q2D turbulent instabilities are suppressed.

The selection of the Grashof number is associated with the Lykoudis number $Ly = Ha^2/Gr^{0.5}$ [28], as well as with the transition criterion from forced to mixed (or natural) convection (Re^2/Gr) as explained in [29]. The 3D case studied in [18] that showed a fully developed behaviour was defined by $Ly = 8.3$ and $Re^2/Gr = 8.3$. Raising the Ha up to ~ 3000 enhances the stability associated to the Ly while decreasing the Re reduces the stability associated to the force convection assessed by the Re^2/Gr ratio. The selected maximum Gr number has been 10^7, which allows certain mixed convection ($Re^2/Gr = 0.9$) while it guarantees the magnetic dumping with a $Ly \sim 3 \cdot 10^3$.

In the latest DCLL design, the $Re^2/Gr \sim 10^{-4}$ and the Lykoudis number is $\sim 10^2$. This suggests that the natural convection will dominate the flow and also that the magnetic dumping will be high enough to stabilize it.

Although the latest DCLL design suggests a very small heat flux in the front walls ($GrR \sim 0.001$) this study uses one order of magnitude higher to amplify the effect of the wall of interest on the buoyant flow.

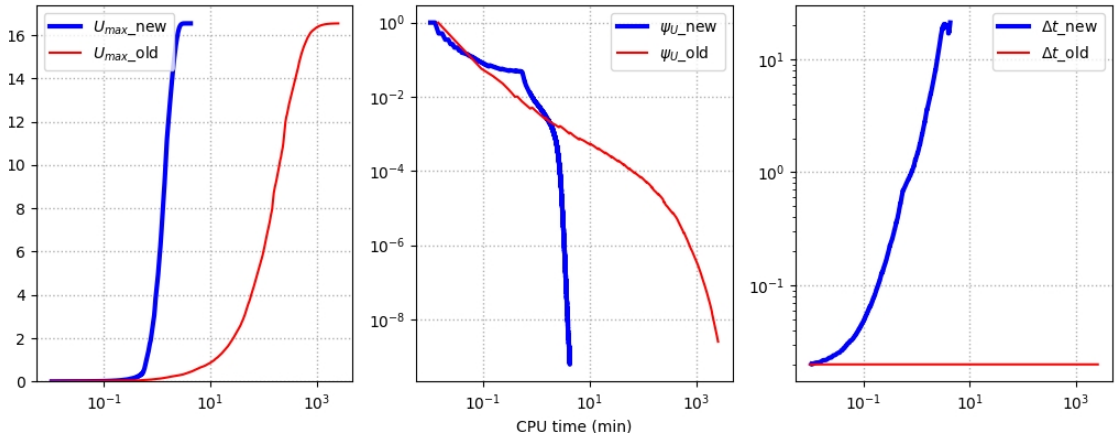

Figure 6: Comparison of old code and new code for $Ha = 100$ and $Gr = 10^4$. Dimensionless maximum velocity (left), variation of the maximum velocity (center) and time step size (right)

The lowest wall conductance ratio (c_w) has been chosen to be that of the SiC wall material, and the highest has been chosen to be four orders of magnitude higher. As the results will show, this four orders of magnitude had no effect on the flow behaviour as the wall still behaves as fully insulating.

The combination of all possibilities gives $2^5 = 32$ cases.

	Ha	Re	Gr	GrR	c_w
High value	3000	3600	1e7	0.02	1e-12
Low value	2400	3000	5e6	0.01	1e-16

Table 4: Selected set of dimensionless variables to generate the combination of cases

The Ha number determines the external magnetic field intensity. The Re determines the averaged flow velocity. The Gr determines the ΔT, and therefore the exponential coefficients. The GrR determines the fixed θ gradient in the right hand side wall boundary. Finally the c_w determines the SiC wall electric conductivity.

The DCLL blanket configuration is somewhat different from the benchmark. Besides the fact that it considers a multi-material problem, the DCLL temperature gradient is originated by a non-uniform volumetric heating caused by the neutron flux interaction.

The parameters of interest analyzed in this work have been:

(1) The Nusselt number, defined as $Nu = h \cdot a/k$ with h the heat transfer coefficient calculated as $h = Q_W/(A_{bw} \cdot \Delta T_{bw})$. ΔT_{bw} is defined as $\Delta T_{bw} = \overline{T}_b - \overline{T}_{bw} = \overline{\theta}_{bw}$. A_{bw} is the area of the interface between bulk and wall in the "wall of study", that can be seen in Figure 7. $\overline{T}_b$ is the mean temperature in the bulk 2D plane, $\overline{T}_{bw}$ is the mean temperature of the "wall of study" and Q_{bw} is the heat flux through the same surface (refer to Figure 7): $Q_{bw} = \int_f k \cdot \nabla\theta_f \cdot \delta A_f$. The area of each discretized face is A_f and $\nabla\theta_f$ is the temperature gradient in such face. Nusselt number is dimensionless.

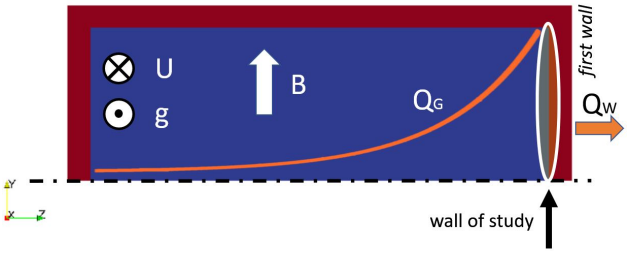

Figure 7: Wall of study

(2) The maximum vorticity throughout the fluid region has been normalized as $\omega_{max} = max(\omega)/U$. Maximum vorticity, after normalization has units of m^{-1}.

(3) The maximum velocity has been defined as the maximum velocity magnitude throughout the fluid region and later normalized as $U_{max} = max(|\mathbf{v}|)/U$. Maximum velocity after normalization is dimensionless.

(4) The maximum theta (θ) in the fluid region. It has units of K or $°C$.

(5) The maximum theta (θ) in the wall region. It has units of K or $°C$.

(6) The maximum theta gradient magnitude ($|\nabla\theta|$) in the wall region. It might be of interest for stress analysis. It has units of K/m or $°C/m$.

(7) The dimensionless pressure drop coefficient (k_p). It is defined as $k_p = (\partial p/\partial x)/(\sigma \cdot U \cdot B^2)$, where $\partial p/\partial x$ is the necessary explicit pressure gradient source term to keep the desired U. The k_p coefficient is dimensionless.

The 32-simulation runs took approximately 8 weeks to finish running in 12 cores in parallel. The cases with $Ha = 3000$ had ~ 150000 nodes in the fluid region and ~ 122000 in the wall region. The cases with $Ha = 2400$ had ~ 133000 and ~ 107000 nodes in fluid and wall region respectively.

Each of the 32 simulations yielded a full 2D-solution of the buoyant fully developed MHD flow. An example of one velocity field can be observed in Figure 8, while Figure 9 shows the difference of dimensionless velocity profiles for

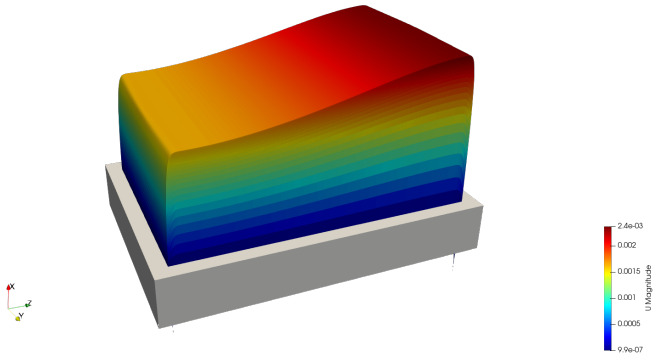

Figure 8: Velocity profile (m/s) in the case with $Ha = 3000$, $Re = 3000$, $Gr = 1e7$, $GrR = 0.02$ and $c_w = 1e-12$

different Gr numbers. In Figure 10 the electric current (j) vectors are shown over an electric potential field. The buoyant phenomenon produces a deviation in the electric current direction close to the first wall.

The purpose of the sensitivity analysis is to find out the influence of the variables on the parameters of interest. Such influence is represented as linear coefficients in a polynomial equation for each of the parameters of interest, and is also represented in the histogram figures with normalized partial derivative as:

$$\frac{\partial Parameter}{\partial Variable} \simeq \frac{\frac{\overline{Param_2} - \overline{Param_1}}{\overline{Param_2}}}{\frac{Var_2 - Var_1}{Var_2}} \tag{7}$$

where $\overline{Param_x}$ is the mean of the 16 values of a parameter of interest characterized by the dimensionless variable (Var_x). The variations have been normalized because the resultant gradients without normalization were different by several orders of magnitude. For example GrR variation is of the same order of magnitude while the difference in the c_w is of the order of $\sim 1e-12$. The expressions of linear dependence for each parameter with respect to the variables in the range of study will be shown in the following discussion. The dependence is linear in this study since only two values for each variable are considered. This does not imply at all that the real relationship is linear. The influence of c_w has been removed from the polynomial expression since both wall electric conductivities result in the same flow regime.

(1) Nusselt number is found to be fairly affected by the four first variables. In Figure 12, the relative variation of the Nusselt number is represented versus the relative variation of the dimensionless variables.

A curious effect can be observed when analyzing the Nusselt number results and the temperature distribution. By definition $Nu \propto Q_{bw}/\theta_W$. Although through the wall of study heat goes out of the fluid domain (liquid next to the wall is hotter than the solid wall), the mean wall temperature is higher than the mean fluid temperature. This can be observed in Figure 11. This is why the Nusselt number

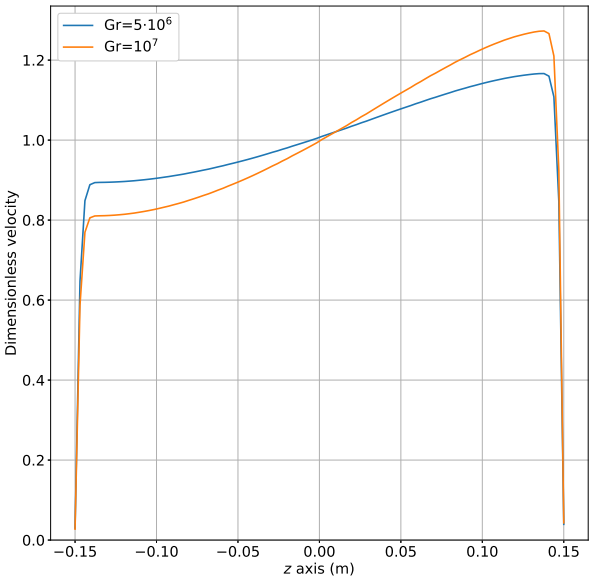

Figure 9: Dimensionless velocity profile in the case with $Ha = 2400$, $Re = 3000$, $GrR = 0.01$ and $c_w = 1e-12$ with different Gr numbers

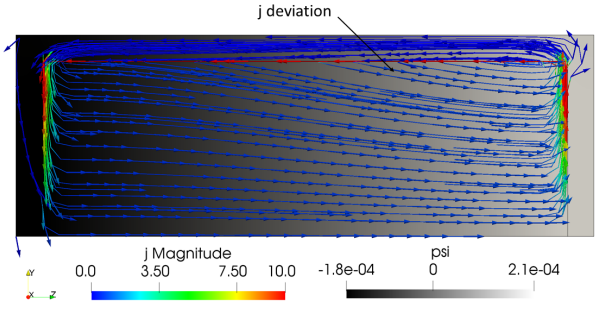

Figure 10: Electric currents and electric potential fields in the case with $Ha = 3000$, $Re = 3000$, $Gr = 1e7$, $GrR = 0.02$ and $c_w = 1e-12$

results are negative in all cases.

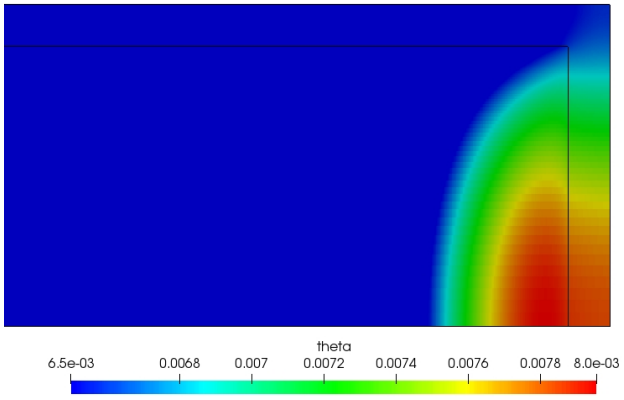

Figure 11: Temperature difference (θ in $^{\circ}C$ or K) distribution in the case with $Ha = 3000$, $Re = 3000$, $Gr = 1e7$, $GrR = 0.01$ and $c_w = 1e-16$

The linear relationship for the Nusselt number is:

$$\mathrm{Nu} = -3.55\cdot10^{-1} + 2.05\cdot10^{-5}\cdot\mathrm{Ha} + 1.57\cdot10^{-5}\cdot\mathrm{Re} - 6.98\cdot10^{-9}\cdot\mathrm{Gr} - 5.91\cdot\mathrm{GrR} \quad (8)$$

The most influencing factor in case of the Nusselt number is the Grashof ratio (GrR) variable. Nusselt value decreases (becomes more negative) as the Grashof ratio gets higher, since Q_W increases in magnitude and $\overline{\theta}_{bw}$ decreases. The same negative tendency is observed for an increase in the Grashof number.

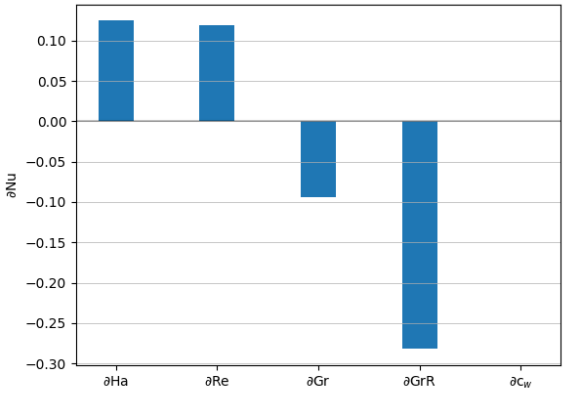

Figure 12: Relative variation of the Nusselt number versus the relative variation of each studied variable

(2) Maximum vorticity (see Figure 13) results in the following expression:

$$\omega = 1.74\cdot10^{3} + 4.98\cdot\mathrm{Ha} - 5.19\cdot10^{-1}\cdot\mathrm{Re} + 2.35\cdot10^{-4}\cdot\mathrm{Gr} - 2.95\cdot10^{3}\cdot\mathrm{GrR} \quad (9)$$

It is mostly affected by variations in the Ha number, followed by Gr and Re. The last one affects it negatively. Maximum vorticity for 2D flows happens in the steepest velocity gradients. It makes sense that higher Ha and higher Gr enhance velocity gradients in the boundary layers. An increase in Re increases inertia forces, and it tends to relocate velocity in the central region, reducing the steepness of the velocity gradients in the walls.

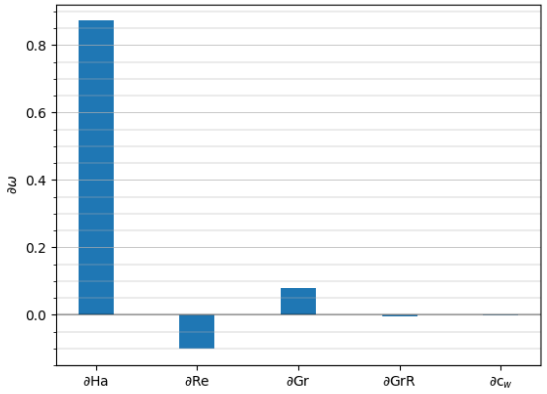

Figure 13: Relative variation of the normalized vorticity (m^{-1}) versus the relative variation of each studied variable

(3) Maximum velocity (Figure 14) results in the expression:

$$\mathrm{U}_{max} = 1.33 - 5.37\cdot10^{-5}\cdot\mathrm{Ha} - 4.11\cdot10^{-5}\cdot\mathrm{Re} + 1.87\cdot10^{-8}\cdot\mathrm{Gr} - 2.51\cdot10^{-1}\cdot\mathrm{GrR} \quad (10)$$

The tendency of the results is logical: increasing Ha flattens the velocity profile and thus gets a lower maximum velocity for a given Re. Increasing Re number decreases maximum velocity. This can be realistic given that maximum velocity is normalized in these simulations and that higher inertia forces can flatten the velocity profile when relevant buoyant forces take place. Increasing Gr again increases maximum velocity, which makes sense because the higher the Gr, the more tilted the velocity profile is and the hot side reaches a higher velocity.

Influences in the maximum temperature difference resulted similar between **(4) bulk** and **(5) wall** (Figure 15), being the GrR effect in the wall domain slightly more important than in the bulk. As expected, Gr number shows the most notable effect in these parameters, and both Ha and Re appear non-negligible in this aspect.

The linear relationship for the maximum temperature difference in the bulk, θ, results in:

$$\theta = -1.56\cdot10^{-3} + 5.71\cdot10^{-7}\cdot\mathrm{Ha} + 4.98\cdot10^{-7}\cdot\mathrm{Re} + 6.39\cdot10^{-10}\cdot\mathrm{Gr} - 1.22\cdot10^{-2}\cdot\mathrm{GrR} \quad (11)$$

whereas the expression for the maximum temperature dif-

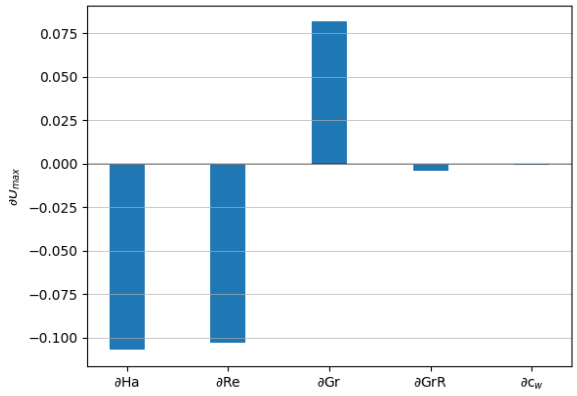

Figure 14: Relative variation of the normalized maximum velocity versus the relative variation of each studied variable

ference in the wall, θ_W, is:

$$\theta_W = -1.50\cdot10^{-3} + 5.59\cdot10^{-7}\cdot\mathrm{Ha} + 4.91\cdot10^{-7}\cdot\mathrm{Re} + 6.32\cdot10^{-10}\cdot\mathrm{Gr} - 1.40\cdot10^{-2}\cdot\mathrm{GrR} \quad (12)$$

(6) Maximum temperature gradient, $\nabla\theta_W$, results in the expression:

$$\nabla\theta_W = -1.42\cdot10^{-2} + 5.02\cdot10^{-6}\cdot\mathrm{Ha} + 3.81\cdot10^{-6}\cdot\mathrm{Re} + 5.81\cdot10^{-9}\cdot\mathrm{Gr} - 6.96\cdot10^{-2}\cdot\mathrm{GrR} \quad (13)$$

It is also similar to the previous two parameters (see Figure 16), with the difference of a marginal higher influence of Re with respect to Ha number.

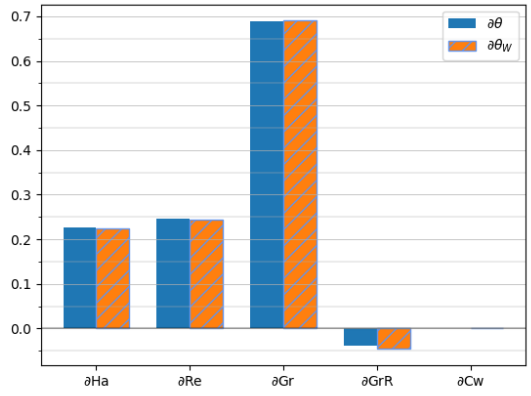

Figure 15: Relative variations of the bulk temperature difference and the wall temperature difference ($°C$ or K) versus the relative variation of each studied variable

(7) Dimensionless pressure drop coefficient kp shows a linear relationship such as:

$$\mathrm{k}_p = 1.56\cdot10^{-3} - 2.93\cdot10^{-7}\cdot\mathrm{Ha} - 4.46\cdot10^{-9}\cdot\mathrm{Re} + 1.94\cdot10^{-12}\cdot\mathrm{Gr} - 1.15\cdot10^{-5}\cdot\mathrm{GrR} \quad (14)$$

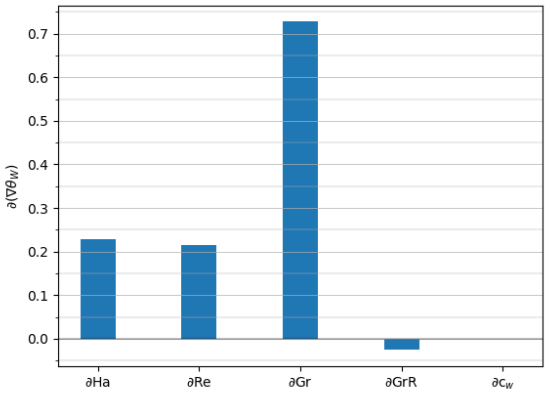

Figure 16: Relative variation of the wall temperature gradient ($°C/m$ or K/m) versus the relative variation of each studied variable

It is highly dependent on the Ha number as expected given its tendency ($1/Ha$). The higher Ha number the lower the kp value, as explained in [30] for insulating channels.

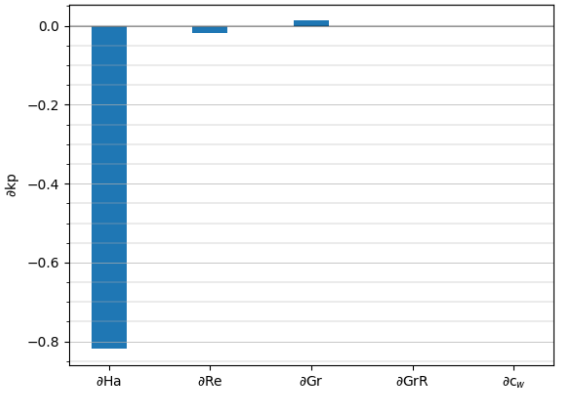

Figure 17: Relative variation of the dimensionless pressure drop versus the relative variation of each studied variable

The sensitivity analysis, though limited to the range of studied values, provides a useful insight on the order of magnitude of the sensitivity of each of the parameters of interests to the chosen dimensionless variables, helping identify the most influencing among the latter.

The results indicate the negligible influence of the c_w in the range of values analyzed. They also indicate the very high influence of the Gr number in all variables associated with θ. Vorticity and dimensionless pressure drop is highly affected by the Ha number. Nusselt number and maximum velocity are influenced in a similar order of magnitude by the differences studied in GrR, Ha, Re and Gr number.

An interesting result that may be open for debate is the validity of the standard definition of the Nusselt number in the type of cases studied in this work. The temperature distribution shows a higher temperature on the wall of in-

terest than the average temperature of the fluid. Since the fluid next to the wall is hotter than the wall, it causes a negative value of the Nusselt number. With the appropriate set of variables, average temperature on the fluid and on the wall may result on the same value, showing an infinite Nusselt number. The physical interpretation of such result would be confusing.

The multi-material ϕ-MHDFoam code has demonstrated to be a powerful tool to capture the fully-developed buoyant MHD phenomenon. The method to generate the 32 cases of interest for the parametric scan has been automated for this work. Future access to HPC resources will easily allow to expand the number of simulations to run. With a large number of simulations, results can be correlated and further used by DCLL engineers in preliminary designs.

6. Conclusions

The buoyant fully developed ϕ-MHDFoam [20] has been successfully validated with a benchmark case [9]. It has been adapted to multi-region cases and has been applied successfully to the latest EU-DCLL design proposal.

The code performance has been optimized and simulations with the new code run orders of magnitude faster while guaranteeing accuracy.

A sensitivity analysis has been carried out through a set of 32 simulations in order to analyze the influence of 5 dimensionless variables (Ha, Re, Gr, GrR and c_w) that characterize the case on 7 parameters of interest (Nusselt number, maximum vorticity, maximum velocity, maximum temperature in the bulk and in the wall, maximum temperature gradient in the solid wall and dimensionless pressure drop coefficient (kp)).

The increase of Re and Ha tend to reduce the steepness of the velocity profile and the vorticity, and reduce temperature differences. Increasing the Gr enhances steepness in the flow profile and in the temperature field. The conclusions are aligned with the observations made in the recent work by Rhodes et. at. [19]. The influence of the selected variables over the temperature gradients of the ceramic walls have been found out for the first time in a buoyant MHD analysis.

The range of values in which the fully-developed assumption applies is still uncertain. Future investigations (currently under development in our group) will clarify under which combination of dimensionless parameters the buoyant MHD flow regime may be considered 2D and fully developed. In future works, the 2D fully-developed approach will be applied for dimensionless parameters closer to the limits of the validity of such assumption. This research line will help to retrieve heat transfer correlations for system design purposes.

~~More investigations are required in fully-developed and 3D flows to retrieve heat transfer correlations for system design purposes.~~

Acknowledgments

This work has been carried out within the framework of the EUROfusion Consortium and has received funding from the Euratom research and training programme 2014-2018 and 2019-2020 under grant agreement No. 633053. The views and opinions expressed herein do not necessarily reflect those of the European Commission. The authors thank as well the contribution of Associació/Col·legi d'Enginyers Industrials de Catalunya with Fundació Caixa d'Enginyers' financial support.

References

[1] G. Federici, C. Bachmann, L. Barucca, C. Baylard, W. Biel, L.V. Boccaccini, C. Bustreo, S. Ciattaglia, F. Cismondi, V. Corato, C. Day, E. Diegele, T. Franke, E. Gaio, C. Gliss, T. Haertl, A. Ibarra, J. Holden, G. Keech, R. Kembleton, A. Loving, F. Maviglia, J. Morris, B. Meszaros, I. Moscato, G. Pintsuk, M. Siccinio, N. Taylor, M.Q Tran, C. Vorpahl, H. Walden, and J.H. You. Overview of the DEMO staged design approach in Europe. *Nuclear Fusion*, 59, 2019.

[2] G. Federici, L. Boccaccini, F. Cismondi, M. Gasparotto, Y. Poitevin, and I. Ricapito. An overview of the EU breeding blanket design strategy as an integral part of the DEMO design effort. *Fusion Engineering and Design*, 141, 2019.

[3] I. Fernández, Palermo I., F.R. Urgorri, D. Rapisarda, and García. DCLL Design Report 2019. *Eurofusion Internal Report: ENR-PRD.BB.WP4-T008-D001*, 2019.

[4] I. Fernández-Berceruelo, I. Palermo, F.R. Urgorri, A. García, D. Rapisarda, and A Ibarra. Alternatives for upgrading the eu dcll breeding blanket from mms to sms. In *Contributed poster at 31st Symposium on Fusion Technology (SOFT)*, 2020.

[5] I. Fernández-Berceruelo, M. Gonzalez, I. Palermo, F. R. Urgorri, and D. Rapisarda. Large-scale behavior of sandwich-like FCI components within the EU-DCLL operational conditions. *Fusion Engineering and Design*, doi.org/10.1016/j.fusengdes.2018.03.044(March), 2018.

[6] H. Ji and R. Gardner. Numerical analysis of turbulent pipe flow in a transverse magnetic field. *International Journal of Heat and Mass Transfer*, 40(8):1839–1851, 1997.

[7] L. Barleon, U. Burr, K. Mack, and R. Stiegliz. Heat transfer in liquid metal cooled fusion blankets. *Fusion Engineering and Design*, 51-52:723–733, 2000.

[8] N. Morley, S. Smolentsev, L. Barleon, I. Kirillov, and M. Takahashi. Liquid magnetohydrodynamics — recent progress and future directions for fusion. *Fusion Engineering and Design*, 51-52:701–713, 2000.

[9] T. Tagawa, G. Authié, and R. Moreau. Buoyant flow in long vertical enclosures in the presence of a strong horizontal magnetic field. Part 1. Fully-established flow. *European Journal of Mechanics B/Fluids*, 21:383–398, 2002.

[10] G. Authié, T. Tagawa, and R. Moreau. Buoyant flow in long vertical enclosures in the presence of a strong horizontal magnetic field. Part 2. Finite enclosures. *European Journal of Mechanics B/Fluids*, 22:203–220, 2003.

[11] S. Smolentsev, R. Moreau, and M. Abdou. Characterization of key magnetohydrodynamic phenomena in PbLi flows for the US DCLL blanket. *Fusion Engineering and Design*, 83:771–783, 2008.

[12] N. Vetcha, S. Smolentsev, and M. Abdou. Theoretical Study of Mixed Convection in Poloidal Flows of DCLL Blanket. *Fusion Science and Technology*, 56:851–855, 2009.

[13] Joal Sommeria and Renè Moreau. Why, how, and when, MHD turbulence becomes two-dimensional. *Journal of Fluid Mechanics*, 118(April 2006):507–518, 1982.

[14] F. Urgorri, S. Smolentsev, I. Fernández-Berceruelo, D. Rapisarda, I. Palermo, and A. Ibarra. Magnetohydrodynamic and thermal analysis of PbLi flows in poloidal channels with flow channel insert for the EU-DCLL blanket. *Nuclear Fusion*, 58, 2018.

[15] D. Di Giulio, D. Suarez, Ll. Batet, E. Mas de les Valls, and L. Savoldi. Analysis of flow channel insert deformations influence on the liquid metal flow in DCLL blanket channels. *Fusion Engineering and Design*, 157:111639, 2020.

[16] S. Smolentsev, N. B. Morley, and M. Abdou. Magnetohydrodynamic and thermal issues of the SiCf/SiC flow channel insert. *Fusion Science and Technology*, 50, 2006.

[17] Andrei Khodak, Peter Titus, Thomas Brown, and Jonathan Klabacha. Numerical model of dual-coolant lead – lithium (DCLL) blanket. *Fusion Engineering and Design*, 137(November 2016):124–129, 2018.

[18] E. Mas de les Valls, D. Suarez, and Ll. Batet. BB-5.2.2-T002-D002: Magneto-convection in PbLi vertical ducts. Technical report, EUROfusion, 2017.

[19] Tyler J. Rhodes, Gautam Pulugundla, Sergey Smolentsev, and Mohamed Abdou. 3D modelling of MHD mixed convection flow in a vertical duct with transverse magnetic field and volumetric or surface heating. *Fusion Engineering and Design*, 160(May):111834, 2020.

[20] Elisabet Mas de les Valls. *Development of a simulation tool for MHD flows under nuclear fusion conditions*. PhD dissertation, Dept. of Physics and Nuclear Engineering, Universitat Politècnica de Catalunya, 2011.

[21] Ming-Jiu Ni, Ramakanth Munipalli, Neil B Morley, Peter Huang, and Mohamed A Abdou. A current density conservative scheme for incompressible MHD flows at a low magnetic Reynolds number . Part I : On a rectangular collocated grid system. *Journal of Computational Physics*, 227, 2007.

[22] Elisabet Mas de les Valls, L.A. Sedano, L. Batet, I. Ricapito, A. Aiello, O. Gastaldi, and F. Gabriel. Lead–lithium eutectic material database for nuclear fusion technology. *Journal of Nuclear Materials*, 376, 2008.

[23] D. Martelli, A. Venturini, and M. Utili. Literature review of lead-lithium thermophysical properties. *Fusion Engineering and Design*, 138(September 2018):183–195, 2019.

[24] U. Müller and L. Bühler. *Magnetofluiddynamics in Channels and Containers*. Springer-Verlag Berlin Heidelberg, 2001.

[25] Belit Garcinuno, David Rapisarda, Rodrigo Antunes, Marco Utili, Iván Fernández-Berceruelo, Javier Sanz, and Angel Ibarra. The tritium extraction and removal system for the DCLL-DEMO fusion reactor. *Nuclear Fusion*, 58(9), 2018.

[26] Chiara Mistrangelo. Identification of requirements for accurate numerical mhd predictions and task work plan. *Eurofusion Internal Report: WPBB-DEL-D-521-01*, 2014.

[27] S. Smolentsev, S. Badia, R. Bhattacharyay, L. Buhler, L. Chen, Q. Huang, H. G. Jin, D. Krasnov, D. W. Lee, E. Mas De Les Valls, C. Mistrangelo, R. Munipalli, M. J. Ni, D. Pashkevich, A. Patel, G. Pulugundla, P. Satyamurthy, A. Snegirev, V. Sviridov, P. Swain, T. Zhou, and O. Zikanov. An approach to verification and validation of MHD codes for fusion applications. *Fusion Engineering and Design*, 100, 2015.

[28] P. S. Lykoudis. Non-dimensional numbers as ratios of characteristic times. *International Journal of Heat and Mass Transfer*, 33(7), 1990.

[29] E. M. Sparrow, R. Eichhorn, and J. L. Gregg. Combined forced and free convection in a boundary layer flow. *Physics of Fluids*, 2(3), 1959.

[30] L. Barleon, V. Casal, and L. Lenhart. MHD flow in liquid-metal-cooled blankets. *Fusion Engineering and Design*, 14(3-4):401–412, 1991.